Analysis of a vinculin homolog in a sponge (phylum Porifera) reveals that vertebrate-like cell adhesions emerged early in animal evolution

Received for publication, December 11, 2017, and in revised form, May 21, 2018 Published, Papers in Press, June 7, 2018, DOI 10.1074/jbc.RA117.001325

Phillip W. Miller[‡1], **Sabine Pokutta**[‡§1], **Jennyfer M. Mitchell**[¶], **Jayanth V. Chodaparambil**[‡§], **D. Nathaniel Clarke**[‖], **W. James Nelson**[‡‖], **William I. Weis**[‡§2], **and Scott A. Nichols**[¶3]

From the Departments of [‡]*Molecular and Cellular Physiology and* [§]*Structural Biology, School of Medicine and the* [‖]*Department of Biology, Stanford University, Stanford, California 94305 and the* [¶]*Department of Biological Sciences, University of Denver, Denver, Colorado 80208*

Edited by Karen G. Fleming

The evolution of cell-adhesion mechanisms in animals facilitated the assembly of organized multicellular tissues. Studies in traditional animal models have revealed two predominant adhesion structures, the adherens junction (AJ) and focal adhesions (FAs), which are involved in the attachment of neighboring cells to each other and to the secreted extracellular matrix (ECM), respectively. The AJ (containing cadherins and catenins) and FAs (comprising integrins, talin, and paxillin) differ in protein composition, but both junctions contain the actin-binding protein vinculin. The near ubiquity of these structures in animals suggests that AJ and FAs evolved early, possibly coincident with multicellularity. However, a challenge to this perspective is that previous studies of sponges—a divergent animal lineage—indicate that their tissues are organized primarily by an alternative, sponge-specific cell-adhesion mechanism called "aggregation factor." In this study, we examined the structure, biochemical properties, and tissue localization of a vinculin ortholog in the sponge *Oscarella pearsei* (*Op*). Our results indicate that *Op* vinculin localizes to both cell–cell and cell–ECM contacts and has biochemical and structural properties similar to those of vertebrate vinculin. We propose that *Op* vinculin played a role in cell adhesion and tissue organization in the last common ancestor of sponges and other animals. These findings provide compelling evidence that sponge tissues are indeed organized like epithelia in other animals and support the notion that AJ- and FA-like structures extend to the earliest periods of animal evolution.

This work was supported by National Institutes of Health Grants R35GM118064 (to W. J. N.) and R01GM114462 (to W. I. W.) and NASA Grant 15-EXO15_2-0027 (to W. I. W. and S. A. N.). The authors declare that they have no conflicts of interest with the contents of this article. The content is solely the responsibility of the authors and does not necessarily represent the official views of the National Institutes of Health.

This article contains Tables S1 and S2, Figs. S1–S10, and sequences.

The atomic coordinates and structure factors (code 6BFI) have been deposited in the Protein Data Bank (http://wwpdb.org/).

[1] Both authors contributed equally to this work.

[2] To whom correspondence may be addressed. E-mail: bill.weis@stanford.edu.

[3] To whom correspondence may be addressed. E-mail: scott.nichols@du.edu.

Cell adhesion is widely considered to be a requirement for the evolution of multicellularity (1–3). Cell–cell adhesion molecules connect adjacent cells within tissues (4), and other adhesion molecules anchor cells and tissues to the secreted extracellular matrix (ECM)[4] (5). In addition, cell-adhesion mechanisms have evolved to play important roles in many other aspects of normal tissue physiology and development, including spatial landmarks that help determine cell polarity (6, 7), spindle orientation during mammalian mitotic cell division (8), signaling functions in response to mechanical forces on cells and tissues (9), and dynamic tissue remodeling during cell motility (10, 11). The critical importance of cell adhesion in multicellularity is underscored by the observation that cell adhesion is typically misregulated in cancer (12), a phenomenon unique to multicellular organisms.

Some of the earliest experimental studies of cell adhesion in animals were conducted on sponges (phylum Porifera). In 1907, Wilson (13) famously observed that cells derived from dissociated tissues of sponges could reaggregate and develop into a functional organism. This process relies on a secreted proteoglycan complex termed the aggregation factor (AF) that functions both in cell adhesion and self/nonself recognition (14–18). Core proteins of the AF have been identified and are structurally composed of calx-β domains and a sponge-specific "wreath" domain (19). Sulfated polysaccharide components of the AF undergo calcium-dependent, homophilic interactions that are considered to be the predominant adhesion mechanism in sponges (20).

The AF model of sponge cell adhesion is different from adhesion mechanisms in other animals. Two of the most important animal adhesion structures are the adherens junction (AJ) and focal adhesions (FAs). The AJ anchors adjacent cells to each other, and FAs anchor cells to the secreted ECM. These adhesive structures utilize entirely unrelated transmembrane adhesion proteins: the AJ is predominantly composed of cadherins (21, 22), whereas FAs contain integrins (23). Cadherins anchor to the actin cytoskeleton through a cytoplasmic protein com-

[4] The abbreviations used are: ECM, extracellular matrix; AJ, adherens junction; FA, focal adhesion; AF, aggregation factor; VIN, protein superfamily of α-catenin, α-catulin, and vinculin; *Op*, *O. pearsei*; CAD, cadherin; SEC–MALS, size-exclusion chromatography and multiangle light scattering; ITC, isothermal titration calorimetry.

plex of β-catenin, α-catenin, vinculin, and other proteins; integrins anchor to the actin cytoskeleton through interactions with a large number of cytoplasmic proteins including talin, vinculin, and paxillin (24–28).

Differences between the AF model in sponge cell adhesion and AJ and FA adhesions in other animals have contributed to the view that sponge tissues fall short of the organization level found in epithelia of other animals (29–31). Although this perspective has not gone unchallenged (31–33), there is limited ultrastructural evidence for cell junctions in sponge tissues, and where known they are not defined molecularly (32, 34). Furthermore, most sponges lack an obvious basal lamina (29), the specialized ECM to which epithelial FAs attach. Nevertheless, comparative genomic studies have established that sponges share homologs of core AJ and FA genes with other animals (35–37), and there is some evidence for their conserved biochemical interactions (38), suggesting a much earlier origin for these structures. Indeed, the apusozoan *Amastigomonas* sp. and the close animal outgroup *Capsaspora owczarzaki* have a complete integrin adhesome (39), and homologs of the vinculin/α-catenin family are widespread in eukaryotes including the social amoeba *Dictyostelium discoideum* (40–42). These observations raise questions about whether some form of transient multicellularity might be more ancient within eukaryotes than previously thought (42) and whether AJ and FA proteins have adhesive functions in the immediate animal stem lineage.

Here, we describe the structure and biochemical properties of a vinculin ortholog (*Op* vinculin) from the sponge *Oscarella pearsei*. *O. pearsei* belongs to the clade homoscleromorpha, which may have the most epithelial-like tissues of any sponge group (29, 34, 43–45). Junction-like structures have been detected in the homoscleromorph larval epithelium (46), and adult tissues have a well-developed basal lamina-like structure that contains type IV collagen (43). Additionally, a yeast two-hybrid screen revealed an interaction between *Op* β-catenin and *Op* cadherin (47). To further evaluate the molecular organization of sponge tissues, we examined: 1) the subcellular and tissue localization of vinculin in tissues of *O. pearsei*; 2) a structural comparison between *Op* vinculin and vertebrate α-catenin and vinculin; and 3) the interaction of *Op* vinculin with F-actin, β-catenin and talin, as a test for a role for vinculin in cadherin or integrin-based cell-adhesion mechanisms. Our results indicate that *Op* vinculin is an ortholog of vertebrate vinculin and that its protein-binding partners and subcellular distribution are consistent with potential roles in both AJ- and FA-mediated cell adhesions.

Results

Identification of O. pearsei VIN proteins and possible complex components

The *O. pearsei* genome (47) and transcriptome (48) was found to encode three predicted sequences with homology to the protein superfamily of αE-catenin, vinculin, and α-catulin (VIN-family proteins; Fig. 1). The three *Op* VIN-family proteins clustered with other animal sequences (Fig. 1*A*), consistent with previous studies (40, 71). *Op* vinculin grouped with other animal vinculin sequences, and *Op* α-catenin grouped with other animal α-catenin sequences. A third *Op* VIN-family protein clustered within a clade of functionally uncharacterized VIN-family proteins that appears to be unique to animals and broadly conserved across the major animal groups. It is present in sponges and cnidarians, as well as multiple protostome and deuterostome phyla (*e.g.* molluscs, echinoderms, and invertebrate chordates), but is absent in nonanimal eukaryotes and appears to have been lost secondarily in vertebrates and the common research models *D. melanogaster* and *Caenorhabditis elegans* (40, 71). In *O. pearsei*, this sequence has a vinculin-like D2 domain (Fig. 1*C*), and the clade to which it clustered lacks close affinity with vinculin, α-catenin, and α-catulin, so we refer to this protein as "*Op* uncharacterized."

As an additional measure of similarity, we examined the predicted domain organization between *Op* VIN proteins and their putative orthologs in other animals. Vertebrate vinculins comprise a series of four helix bundles that form domains 1A, 1B, 2A, 2B, 3A, 3B, and 4, followed by a flexible proline rich linker and a C-terminal five-helix bundle that binds F-actin (72–74) (Fig. 1, *B–D*). α-Catenin family proteins have a similar structure but lack domains 2A and 2B (75). In α-catenin, domain 1A (also called N_I) binds to β-catenin (69, 76, 77) and in mammals is the site for homodimerization, which occludes β-catenin binding (69, 75). In vinculin, domain 1A binds talin and mediates autoinhibition of F-actin binding. *Op* vinculin is 31.7% identical to *Mm* vinculin and 23.7% identical to *Mm* αE-catenin (Fig. 1*B*). However, *Op* vinculin lacks domain 2, which typically distinguishes vinculin from α-catenin in other animals and may contribute to the autoinhibition of F-actin binding (Fig. 1*C*). *Op* uncharacterized has a similar sequence identity to both α-catenin and vinculin (23.2 and 22.1% identity, respectively) and has domain 2 (Fig. 1*C*). *Op* α-catenin is most similar to *Mm* αE-catenin and least similar to *Mm* vinculin by sequence (31.8 and 20.3% identity, respectively, for α-catenin) (Fig. 1*B*) and also lacks domain 2.

Next, we tested the possibility of complete, vertebrate-like cell adhesion complexes in *O. pearsei* by searching for homologs of other AJ and FA proteins. We identified the previously described *Op* cadherin homolog (CAD1) and β-catenin (47), a second uncharacterized classical cadherin *Op* CAD2, and *Op* talin (Fig. 1*D*). *Op* CAD1 and 2 have large extracellular regions that contains 25 and 28 CAD repeats, respectively, and both have laminin G and epidermal growth factor-like domains (Fig. 1*D*). In general, cadherins in nonbilaterian animals contain a longer extracellular region with a greater variety of domains compared with vertebrate classical cadherins, which have five CAD repeats and lack laminin G and epidermal growth factor-like domains (40). Like vertebrate classical cadherins, *Op* CAD1 and 2 are single pass transmembrane proteins with a cytosolic catenin-binding region. The domain organizations of *Op* talin and β-catenin are more highly conserved than in VIN proteins or cadherins. As in their mammalian counterparts, *Op* talin has an N-terminal FERM domain followed by a talin middle domain, vinculin-binding sites, and an I/WLEQ domain. Just C-terminal to the FERM domain, *Op* talin also has a predicted phosphotyrosine-binding domain that is not present in mouse talin. Like β-catenin in most vertebrates and invertebrates, *Op*

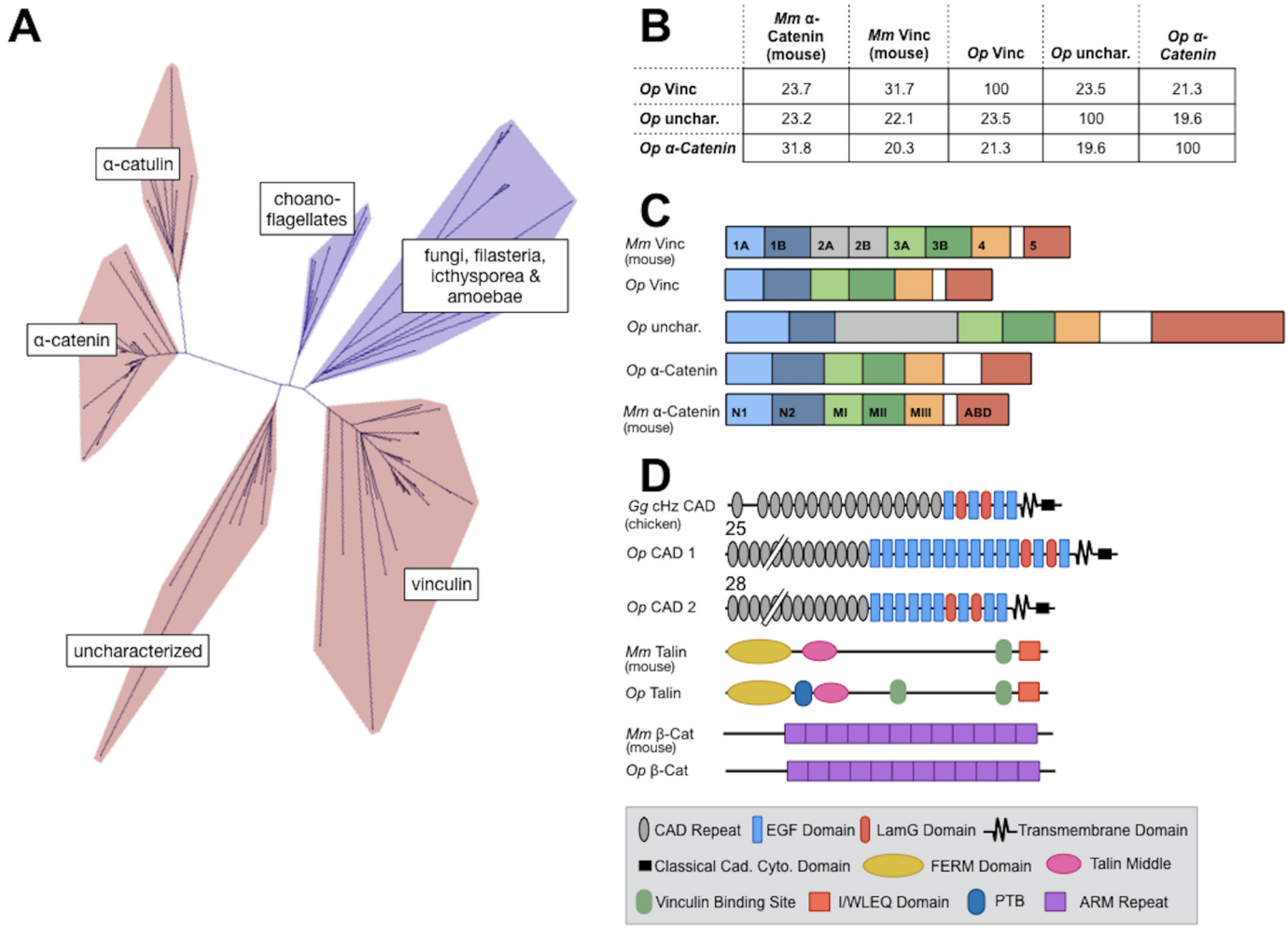

	Mm α-Catenin (mouse)	*Mm* Vinc (mouse)	*Op* Vinc	*Op* unchar.	*Op* α-Catenin
***Op* Vinc**	23.7	31.7	100	23.5	21.3
***Op* unchar.**	23.2	22.1	23.5	100	19.6
***Op* α-Catenin**	31.8	20.3	21.3	19.6	100

Figure 1. VIN homology proteins of the sponge, *O. pearsei*. *A*, unrooted network depicting the phylogeny of VIN-family proteins (*red*, sequences from animal species; *blue*, sequences from nonanimal species). Three VIN-family proteins from *O. pearsei* were found to fall within the animal-exclusive clades corresponding to vinculin, α-catenin, and a functionally uncharacterized clade. A detailed phylogeny is provided in Figs. S1–S7. *B*, the percentage of identity of amino acid sequences of *Mus musculus* αE-catenin (*Mm* α-cat), *Mm* vinculin (*Mm* Vinc), and *Op* VIN proteins. *C*, domain schematics of *Mm* αE-catenin, *Mm* vinculin, and *Op* VIN proteins. *Mm* vinculin is composed of seven 4-helix bundle domains (D1–D4), a proline-rich hinge region (*white*), and a C-terminal 5-helix bundle (D5, the actin-binding domain). Domains 1, 2, and 3 each comprise two 4-helix bundles that share a central, long helix and are therefore subdivided into subdomains A and B. *Mm* αE-catenin shares a similar structure to *Mm* vinculin but lacks domain D2 (*gray*); the N-terminal domain is homologous to vinculin D1, and the M domain comprises three 4-helix bundles equivalent to vinculin D3A, D3B, and D4. The homologous domains in *Op* vinculin, *Op* uncharacterized, and *Op* α-catenin are color-coded. The length of the domain schematics represents the length of the corresponding amino acid sequences. *D*, Pfam-predicted domain composition of potential binding partners of *Op* VIN proteins examined in this study, shown relative to their vertebrate counterparts. Predicted Pfam domains of *Op* CAD1, *Op* CAD2, *Op* Talin, and *Op* β-catenin are annotated in the figure legend. The *numbers* above *Op* CAD1 and *Op* CAD2 indicate the number of extracellular cadherin repeats.

β-catenin is comprised of 12 armadillo repeats flanked by N- and C-terminal regions (47).

Op vinculin co-localizes with F-actin at cell boundaries, at filopodia, and at the base of microvilli in choanocytes

In other animals, VIN family proteins localize to the cell–cell adhesion complex and the FA cell–ECM complex. To characterize tissue-specific and subcellular localization patterns of *Op* vinculin, we isolated a polyclonal antibody against full-length recombinant protein. The affinity-purified antibody predominantly recognized a single band of the predicted size of *Op* vinculin (92 kDa) by Western blotting of whole-cell lysates, and preincubation of the antibody with recombinant protein depleted this signal (Fig. 2*A*). The specificity of the antibody was further validated by immunoprecipitation of endogenous *Op* vinculin from whole cell lysates (Fig. S8).

O. pearsei comprises two types of epithelia: an outer epithelium termed the pinacoderm and a feeding epithelium termed the choanoderm that contains choanocytes (Fig. 2*B*). Immunostaining revealed four distinct *Op* vinculin subcellular distributions within these two epithelia: 1) a belt-like zone at points of cell–cell contact in the pinacoderm (Fig. 2*C*); 2) in filopodial/lamellopodial extensions of motile cells within the mesohyl (Fig. 2*D*); 3) at the base of the microvillar collar of choanocytes within the choanoderm (Fig. 2*E*), a belt-like zone of cell–cell contact in the choanoderm (Fig. 2*F*), and 4) within the cytoplasm of cells in the pinacoderm (Fig. 2*C*) (the pinacoderm is so thin that details of structures associated with vinculin were difficult to resolve in the *z* axis and may correspond to abundant filopodia in this tissue, as shown by transmission EM (48)). In each cellular context, *Op* vinculin appeared to co-localize with actin filaments, indicating an evolutionarily conserved interac-

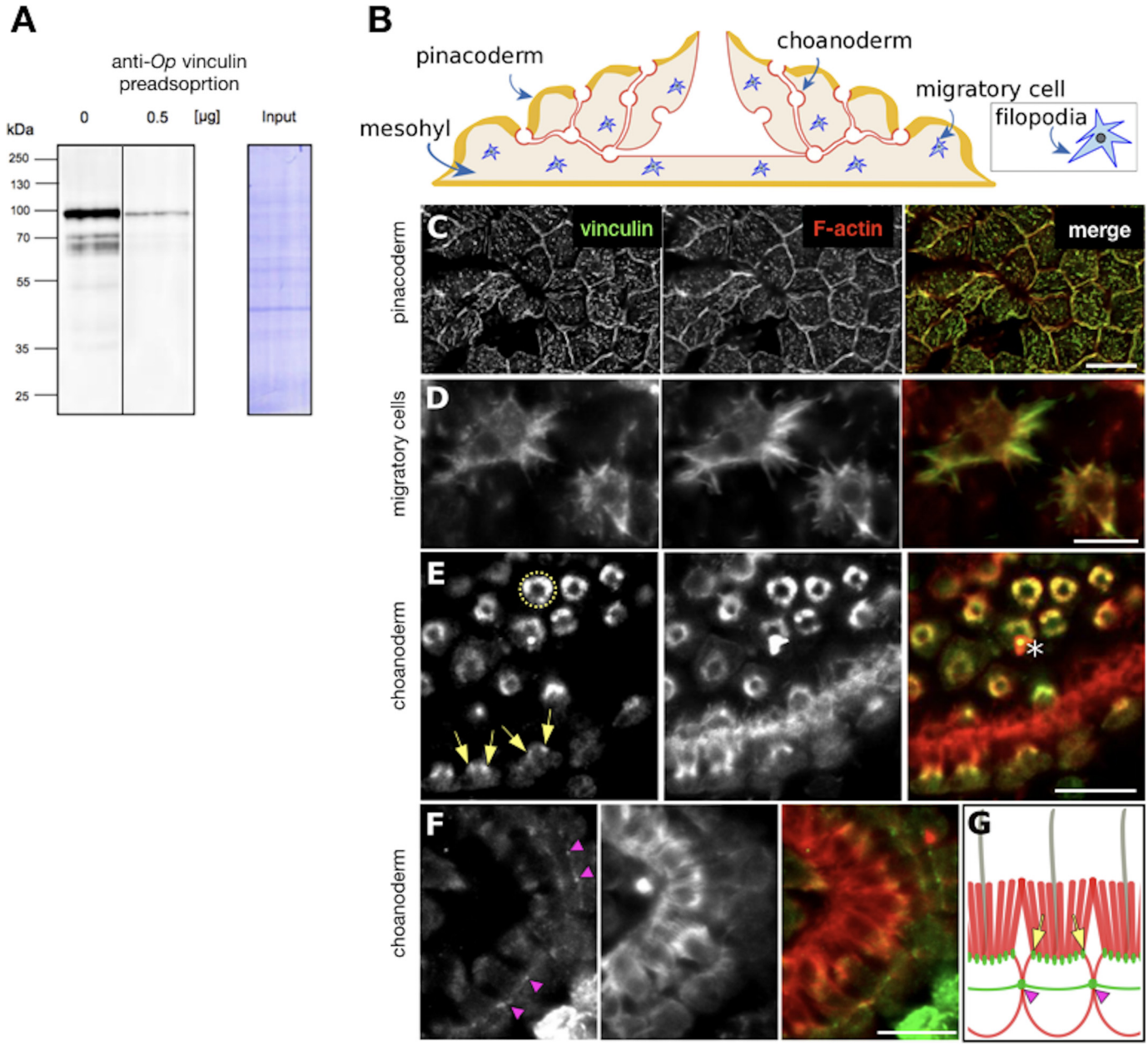

Figure 2. **Specificity of *Op* vinculin antibody and tissue localization of vinculin in *O. pearsei*.** *A*, *O. pearsei* cell lysates probed with antibodies against His-*Op* vinculin in the absence and presence of a competing protein. In the absence of competing protein, the antibody recognizes a single band of ~92 kDa, and faster migrating bands corresponding to degraded *Op* vinculin. Preincubation of the antibody with competing protein 0.5 μg of His-tagged *Op* vinculin reduced binding to *Op* vinculin by >90%. *B*, simplified illustration of the *O. pearsei* body plan. *Op* vinculin localized to the pinacoderm (*yellow*), the choanoderm (*red*), and to migratory cells in the mesohyl (*blue*). *C–F*, tissue and cellular localization of *Op* vinculin by immunostaining at cell– boundaries in the pinacoderm (*C*), filopodia in migratory in the mesohyl (*D*), an F-actin population at the base of microvilli in choanocytes (cross-section views of staining are visible as rings (*hatched yellow circle*) in the *top half* of the panel and longitudinal-section views of staining visible in the bottom half of the panel (*yellow arrows*)) (*E*), and at points of contact between individual choanocytes that form a continuous belt around adjacent cells (*pink arrowheads*) (*F*). *Asterisk* shows a foreign particle (staining artifact). *G*, cartoon summary of choanocyte staining (*green*, vinculin; *red*, F-actin). *Scale bars*, 10 μm.

tion with the actin cytoskeleton. The localization of *Op* vinculin to cell–cell contacts in the pinacoderm and choanoderm is consistent with a possible AJ in these tissues, despite the lack of ultrastructural evidence (35).

Op vinculin is a stable monomer

Despite the phylogenetic placement of *Op* vinculin within the animal vinculin clade and the higher homology of individual *Op* vinculin domains to those of vertebrate vinculin *versus* α-catenin, the absence of a D2 domain and its localization to cell–cell contacts suggested that *Op* vinculin could be functionally closer to α-catenin. Mammalian αE-catenin, but not vinculin, exists as a monomer, homodimer, and heterodimer with β-catenin in epithelial cells, and its oligomerization state regulates its biochemical properties and function in the cell (78, 79). To determine whether *Op* vinculin is exclusively monomeric in solution or whether it also dimerized like mammalian αE-catenin, purified full-length *Op* vinculin was concentrated to 120 μM, incubated at room temperature for 1 h, and analyzed by size-exclusion chromatography and multiangle

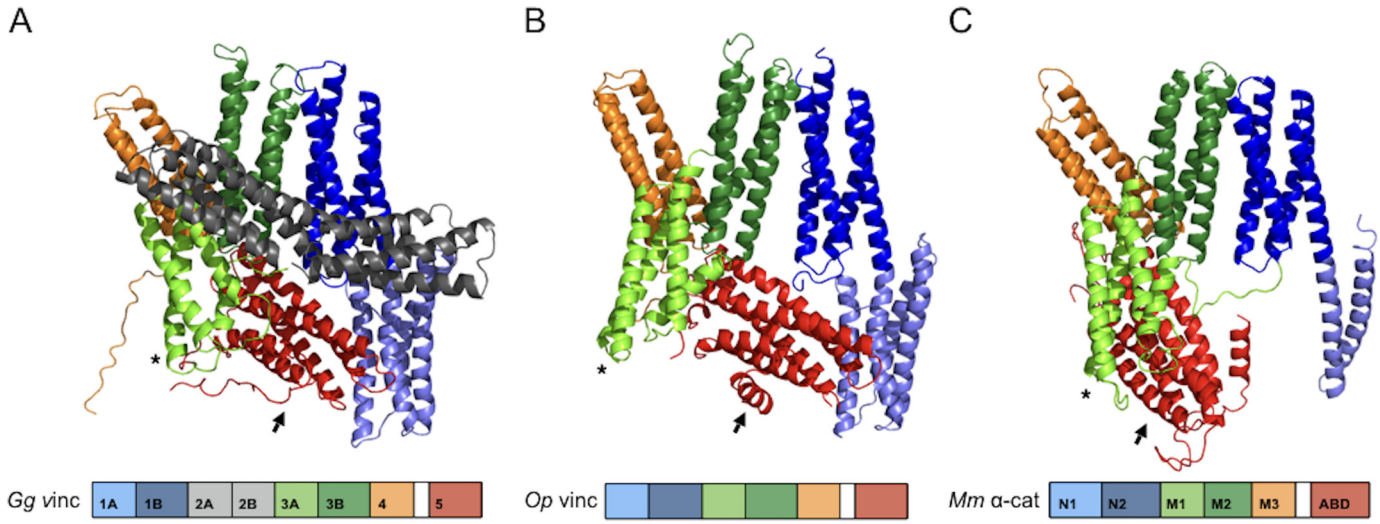

Figure 3. High resolution crystal structure of full-length *Op* vinculin. *A–C*, comparison of *Op* vinculin structure (*B*) with previously solved structures of chicken vinculin (*A*) (73) and subunit B of human αE-catenin dimer (*C*) (75). Domain schematic of each protein is below the structure, and the domains of each protein are color-coded: 1A in *light blue*, 1B in *dark blue*, 2A and 2B in *gray*, 3A in *light green*, 3B in *dark green*, 4 in *orange*, and domain 5/actin-binding domain in *red*. *Asterisks* and *arrows* indicate conformational shifts of domains 3A and 5/actin-binding domain, respectively.

light scattering (SEC–MALS). *Op* vinculin eluted as a discrete peak with an estimated molecular mass of 87.0 kDa by MALS (Fig. S10), which is within 5 kDa of the predicted monomer molecular mass of 91.7 kDa, indicating that it is a monomer in solution, a property of mammalian vinculin but not αE-catenin. It should be noted, however, that some non-mammalian αE-catenins, such as those from *Danio rerio*, *C. elegans*, and *Nematostella vectensis*, are monomeric (71, 80, 81).

High-resolution crystal structure of full-length Op vinculin

To investigate further the relationship between *Op* vinculin, vertebrate vinculin, and αE-catenin, we determined the X-ray crystal structure of *Op* vinculin at 2.3 Å resolution (Fig. 3; Table S2). The overall structure of *Op* vinculin (Fig. 3*B*) resembles the structures of *Hs* and *Gg* vinculin (Fig. 3*A*) (64, 73) and a single subunit of *Mm* αE-catenin homodimer (Fig. 3*C*) (75), as expected for proteins in the vinculin/α-catenin superfamily. Differences among these proteins arise in part from the relative positions of the N-terminal and central domains, which appears to be due to a somewhat flexible interface between the D1b/N_{II} and D3b/M_{II} helix bundles.

Inspection of individual structural regions reveals that *Op* vinculin is more similar to vertebrate vinculin than to *Mm* α-catenin. In particular, *Op* vinculin D1 closely matches vertebrate vinculin D1: subdomains D1a and b are in virtually identical positions, and the long helix that is shared between the subdomains is similarly kinked. Moreover, the fourth helix of subdomain D1a is noticeably curved in vertebrate vinculin and *Op* vinculin. These features are absent in the equivalent region of *Mm* α-catenins, known as domain N. In the α-catenin homodimer, the first two helices of domain N are disordered, and the second two form the homodimer interface with those in the partner molecule (75). A monomeric structure of domain N from αN-catenin, an isoform of αE-catenin that is expressed predominantly in neuronal cells, shows that subdomain N_I forms a four-helix bundle (82), but its position differs slightly from that observed in vertebrate vinculin or *Op* vinculin D1a. Thus, whereas the overall structure of D1 is conserved in VIN proteins, the relative positions of the two subdomains differ from vertebrate vinculin and α-catenin.

The central portion of all VIN-family proteins contains three four-helix bundles, designated D3a, D3b, and D4 in vertebrate vinculin and M_I, M_{II}, and M_{III} in α-catenin. In most animals, vinculin orthologs also contain domain D2, which precedes D3. As expected from sequence analysis, D2 is missing in *Op* vinculin (Figs. 1 and 4, *A* and *B*). Domains D3b and D4 of vertebrate vinculin superimpose very closely with M_{II} and M_{III} of α-catenin, and the *Op* vinculin is also very similar in these regions. In contrast to D3b and D4, the position of the *Op* vinculin domain D3a/M_I differs among all three proteins (Fig. 3), although *Op* vinculin domain D3a is closer to that of α-catenin than to vinculin. This is likely due to the absence of domain D2 in *Op* vinculin and α-catenin; vinculin domain D2 interacts extensively with and helps to fix the position of domain D3a (Fig. 3, *asterisks*).

Vertebrate vinculin domain D2 forms a bridge that interacts with domains 1 and 3. This interaction has been proposed to lock vinculin into a closed conformation around the F-actin-binding domain D5 (Fig. 3*A*), which prevents constitutive binding to actin except upon activation by binding to a partner such as talin (83). α-Catenins lack domain D2, and the position of the F-actin-binding domain in the αE-catenin dimer structure is different in the two promoters (75) and is disordered in another crystal structure (83). These observations are consistent with αE-catenin binding to F-actin without prior activation. Despite the absence of domain D2, *Op* vinculin domain D5 is positioned similarly to vertebrate vinculin domain D5. However, the shifted position of D3a produces few contacts with D5 and thereby makes D5 more exposed, with a surface accessibility intermediate between that of the comparable *Mm* αE-catenin and vertebrate vinculin domains (Fig. 3).

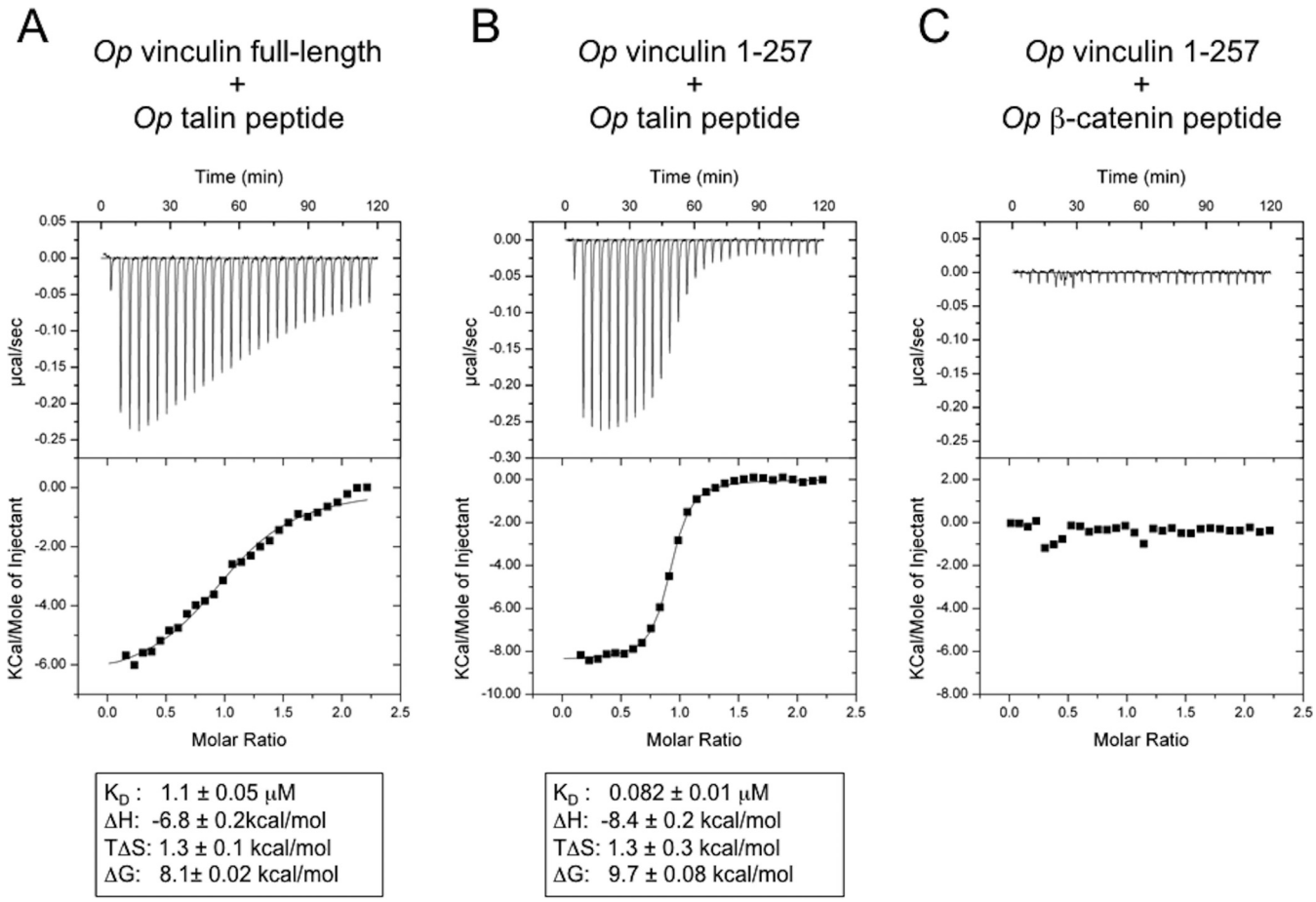

Figure 4. Op vinculin interacts with *Op* talin, but not *Op* β-catenin. The dissociation constants and thermodynamic parameters determined by ITC of *Op* vinculin and different putative binding partners. *A*, full-length *Op* vinculin and a synthetic peptide comprising the vinculin-binding site 1 of *Op* talin (*Op* talin peptide). *B*, *Op* vinculin domain 1 (residues 1–257) and the *Op* talin peptide. *C*, *Op* vinculin domain 1 and a synthetic peptide comprising the α-catenin-binding site on *Op* β-catenin (*Op* β-cat peptide). The data shown represent the averages and the standard deviations of three independent measurements.

Op vinculin binds talin, but not β-catenin

The vinculin-like position of the *Op* vinculin F-actin-binding domain indicates that *Op* vinculin might be autoinhibited with respect to F-actin binding. On the other hand, the relative exposure of this domain might enable it to bind F-actin without prior activation, which is a property of α-catenins. Therefore, we tested whether purified *Op* vinculin bound to talin and/or to β-catenin, and whether binding to F-actin is constitutive or requires activation.

Binding of talin to vinculin is regulated by the intramolecular vinculin head–tail interaction (73, 83, 84), whereas α-catenins bind β-catenin constitutively (85–87). Using isothermal titration calorimetry (ITC), we measured binding of full-length *Op* vinculin and *Op* vinculin D1 to synthetic peptides of *Op* talin and *Op* β-catenin that corresponded to their binding sites on vertebrate vinculin or αE-catenin, respectively (see "Experimental procedures"). Full-length *Op* vinculin and *Op* vinculin D1 bound *Op* talin peptide (Fig. 4, *A* and *B*), but not *Op* β-catenin peptide (Fig. 4*C*). *Op* vinculin D1 bound *Op* talin peptide with K_D = 82 nM (Fig. 4*B*), comparable with mammalian vinculin–talin peptide binding (K_D = 39 nM) (70). In mammalian vinculin, talin binding involves the rearrangement of domain 1A into a five-helix bundle (74), and interactions of D1a with the F-actin-binding domain inhibit detectable talin binding (73). Full-length *Op* vinculin bound to the *Op* talin peptide with K_D = 1.1 μM, *i.e.* > 10-fold reduced affinity for the full-length protein (Fig. 4*A*). These data suggest that *Op* vinculin functions as vinculin, including autoinhibitory behavior likely caused by the D1–D5 interaction, although the autoinhibition is not as strong as that found in vertebrate vinculin.

Op vinculin binding to F-actin is activated by talin

The similarity in the tertiary structures of *Op* vinculin and vertebrate vinculin, as well as the partial autoinhibition of full-length *Op* vinculin binding to talin, led us to examine the F-actin-binding properties of *Op* vinculin using a co-sedimentation assay (81, 85, 88). Like vertebrate vinculins, *Op* vinculin did not bind F-actin significantly above background at concentrations up to 15 μM (Fig. 5, *A* and *C*).

The interaction between the head domain and the ABD domain in mammalian vinculin is disrupted upon binding to talin, which results in activation of vinculin binding to F-actin (74, 83). In the presence of *Op* talin peptide, full-length *Op* vinculin bound to F-actin filaments (Fig. 5, *B* and *C*). Thus, binding of talin to *Op* vinculin D1 releases autoinhibition for F-actin binding, similar to the behavior of vertebrate vinculin.

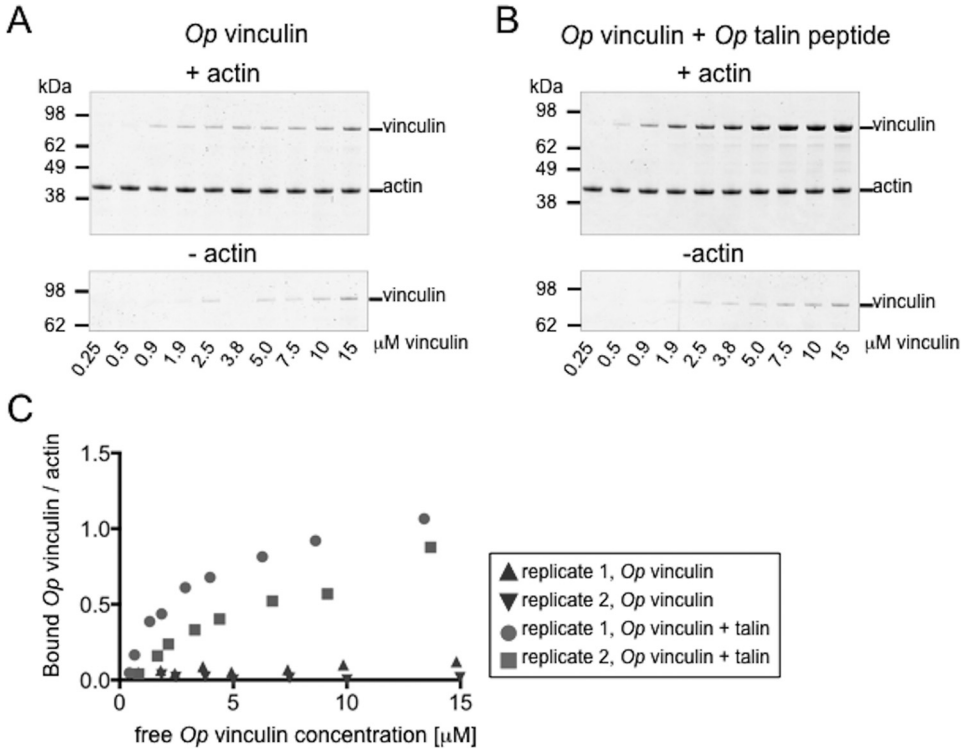

Figure 5. Activation of *Op* vinculin binding to F-actin by *Op* talin. *A* and *B*, *Op* vinculin co-sedimentation with F-actin in the absence (*A*) or presence (*B*) of the *Op* talin peptide. *Op* vinculin was added at increasing concentrations to 1.5 μM F-actin. Background *Op* vinculin pelleting in the absence of F-actin is shown in the *lower panels*. *Op* talin peptide was used in 5-fold excess to *Op* vinculin. The assay was performed in duplicate. *C*, bound *Op* vinculin/actin plotted against the concentration of free *Op* vinculin concentration is shown for binding without (*triangles*) or with (*circles* and *squares*) the *Op* talin peptide.

Discussion

VIN proteins link actin filaments to membrane proteins at the plasma membrane and are found in all animals and their close outgroups (choanoflagellates, chytridomycetes, apusozoa, amoebozoa) (40, 71). Animal VIN proteins are subdivided into four protein families based on sequence homology: vinculin, α-catenin, α-catulin, and a functionally uncharacterized clade previously called "α-catenin-like" (Fig. 1*A*) (40, 71).

Vinculin and α-catenin have been studied structurally and biochemically *in vitro* and *in vivo*. Mammalian vinculin predominantly localizes to cell–ECM contacts, where it anchors FA complexes to the actin cytoskeleton (23). The N-terminal domain D1 of vinculin binds talin, and the C-terminal domain binds F-actin (83); these binding sites, however, are masked by strong head–tail interactions that are stabilized by domain 2, which locks vinculin in an autoinhibited conformation (73). Vinculin binding to F-actin is activated by binding to talin or another protein (89). In contrast, homodimeric *Mm* αE-catenin binds F-actin constitutively, but F-actin binding by αE-catenin monomer in the cadherin complex is significant only when the complex is subjected to mechanical force (88, 90). Vinculin also associates with cell–cell adhesion AJ complexes, which also requires mechanical force (91, 92).

In invertebrate animals, vinculin has been studied in *C. elegans* and in *D. melanogaster*. In *C. elegans*, the vinculin ortholog DEB-1 is involved in integrin-based cell–ECM adhesions and is a component of the dense body, an anchoring structure in muscles similar to the vertebrate Z-disc. Disruption of DEB-1 function leads to disorganized muscles and paralyzed embryos and is lethal (93–96). In contrast, *D. melanogaster* vinculin is nonessential (97), but constitutive activation caused the formation of abundant cytoplasmic adhesion complexes with talin, producing morphological defects and death (97, 98). Biochemical differences between vertebrate and invertebrate α-catenin have been detailed elsewhere (40, 99), but all α-catenins characterized to date bind β-catenin and F-actin at the AJ and developmental disruption of α-catenin leads to morphological abnormalities and death (80, 100–102).

The *O. pearsei* genome encodes three VIN-family proteins: vinculin, α-catenin, and a member of the uncharacterized animal VIN-family clade (Fig. 1, *A–C*). *Op* vinculin is more similar to bilaterian vinculin than αE-catenin by sequence (32 and 24%, respectively) and would be classified as vinculin using phylogeny-based orthology assignment. However, it lacks domain 2, which is a characteristic of vinculin orthologs in other animals (Fig. 1*C*). *Op* uncharacterized is similar to α-catenin and vinculin by sequence (23 and 22%, respectively) and contains domain 2. The biochemical properties and cellular functions of these proteins have not been investigated in any organism. *Op* α-catenin is significantly more similar to α-catenin than vinculin (32 and 20%, respectively). However, given the uncertainty surrounding the function of *Op* vinculin and *Op* uncharacterized, we are unable to make assumptions about the specific cellular functions of any VIN proteins in *O. pearsei*. We focused our studies on *Op* vinculin to begin to dissect the functional relationship between VIN-family proteins in *O. pearsei*.

Immunofluorescence of *O. pearsei* tissue using an affinity-purified antibody raised against *Op* vinculin showed co-local-

ization with cortical belts of actin filaments at cell– cell contacts in the pinacoderm and choanoderm tissues (Fig. 2, *C–F*) and in filopodial extensions in migratory cells within the mesohyl. Localization to cortical actin at the AJ is a function of αE-catenin in cell– cell adhesion, whereas localization to FAs in filopodia supports cell–ECM adhesion during migration. However, this strict interpretation is confounded by the contractile nature of sponge tissues (103), and the recruitment of vinculin to mammalian AJ under mechanical tension, which may stabilize the cadherin– catenin complex (104). Thus, we examined *Op* vinculin *in vitro* to test whether it might have properties of an α-catenin or vinculin homolog.

Purified recombinant *Op* vinculin was a stable, monomeric protein with an overall structure more similar to vertebrate vinculin than α-catenin (Figs. 3 and 4). Moreover, *Op* vinculin bound talin but not β-catenin (Fig. 4) and displayed a significant level of autoinhibition with respect to talin binding. Finally, *Op* vinculin was constitutively autoinhibited in F-actin binding, but this autoinhibition was relieved by binding talin. Collectively, these characteristics strongly suggest that *Op* vinculin is functionally more similar to vinculin rather than α-catenin, despite the absence of domain D2 that is characteristic of vinculin in other animals.

The presence of *Op* vinculin at both cell– cell and cell–ECM contacts supports the hypothesis that *Op* vinculin may function at both the cadherin-based AJ and integrin-based FAs by reinforcing anchorage to the underlying actin cytoskeleton. Given the tension-dependent association of mammalian vinculin with α-catenin at cell– cell junctions, we cannot exclude the possibility that *Op* vinculin associates with another VIN protein family member under tension at the cadherin– catenin complex. In light of these findings, future investigation of *Op* uncharacterized and α-catenin will be of particular interest. In the *O. pearsei* transcriptome, all three VIN proteins are highly expressed in adult tissues (48). Biochemical characterization will determine whether they have functional redundancy and compete with each other for association with binding partners at FA or AJ or have been co-opted for other functions.

Our results have important implications for the evolution of cell-adhesion mechanisms and the organization of sponge tissues. First, they support the hypothesis that a simple epithelium was part of the shared inheritance of all animal lineages. Second, the AF model of sponge cell adhesion appears to be incomplete, and sponge tissues are organized more like the epithelia in other animals than previously thought. One caveat to this interpretation is that *O. pearsei* belongs to the clade homoscleromorpha, which lacks clear orthologs of the core AF protein family characterized from demosponges (Ref. 19); but see Ref. 105); adhesion mechanisms may differ between modern sponge lineages, which underwent very ancient divergences (106). Alternatively, the AJ and FAs may regulate sponge epithelial organization, whereas AF predominantly functions during reaggregation of dissociated tissues and in histocompatibility reactions, which are the contexts in which the AF has been studied predominantly. Finally, the AF and AJ/FA adhesion systems may also interact. The putative AF receptor (107) has an RGD motif typical of ECM proteins that could facilitate interactions with integrins, thereby coupling these otherwise distinct adhesion mechanisms (30). Nevertheless, based on our studies of *Op* vinculin, we conclude that a complex toolkit of cell adhesion proteins and the rudiments of epithelial organization were already established in the last common ancestor of sponges and bilaterians.

Experimental procedures

Identification of O. pearsei VIN proteins and potential binding proteins

Annotated sequences of α- and β-catenin, vinculin, talin, and E-cadherin orthologs from representative bilaterian species were retrieved from Uniprot databases and used to conduct a BLAST search against the *O. pearsei* genome (47). The predicted sequences were then verified by BLAST search for predicted peptides against the *O. pearsei* transcriptome (48) to recover full-length coding sequences (Table S1). Domain composition of putative *O. pearsei* sequences was predicted using the HMMER and SMART web servers to annotate conserved domain motifs from the Pfam database (49–51). Protein characteristics (molecular mass, theoretical pI, extinction coefficient) were predicted using the ProtParam tool on the ExPASy server (52). An annotated alignment of vinculins is provided in Supplement 2.

Molecular phylogenetics

The NCBI PSI-BLAST server (53) was used to create a position-specific scoring matrix from an alignment of α-catenin, vinculin, and α-catulin sequences (54) in the model organism (landmark) database at NCBI. The position-specific scoring matrix was then used to search the proteome of representative animal and nonanimal species using the standalone version PSI-BLAST as implemented by the NCBI BLAST+ package (version 2.7.1) (55). Specifically, the predicted proteome (derived from either genome of transcriptome data) was searched for *D. discoideum*, *C. owczarzaki*, *Monosiga brevicollis*, *Salpingoeca rosetta*, *Salpingoeca urceolata*, *Codosiga hollandica*, *Salpingoeca dolichothecata*, *Savilla parva*, *Diaphanoeca grandis*, *Trichoplax adhaerens*, *O. pearsei*, *Ephydatia muelleri*, *N. vectensis*, *C. elegans*, *D. melanogaster*, *Strongylocentrotus purpuratus*, *Branchiostoma floridae*, *Lottia gigantea*, and *Capitella teleta*. Significant hits were combined with sequences from Miller *et al.* (40), aligned with ClustalW (40, 54) and trimmed with TrimAl (−gappyout) (56) using the phylogenetics server Phylemon-2 (57). Maximum likelihood model selection was performed using the ModelFinder (AIC selection criterion) (58) as implemented on the IQ-TREE web server (59). The best model (LG+G4+F) was implemented locally using IQ-TREE (v1.6.3) (60) with 1000 ultrafast bootstrap replicates (61), and the resulting trees were visualized using CLC Main Workbench 7 (Qiagen). Initial analyses revealed that some representative sequences from *Mnemiopsis leidyi*, *Allomyces macrogynus*, *Acanthomoeba castellanii*, *Schistosoma mansoni*, and *Clonorchis sinensis* were reconstructed as being exceptionally long branches. Thus, these sequences were removed from the data set, and all analyses were repeated.

Op vinculin antibody production and Western blotting analysis

Anti-*Op* vinculin polyclonal antibodies were generated in rabbits. The coding region from *O. pearsei* cDNA was amplified by PCR, and the product was cloned into the pET28a+ (Novagen) expression vector to generate an in-frame fusion between *Op* vinculin (MG852025) and an N-terminal hexahistidine tag (His-*Op* vinculin). *Op* vinculin was expressed in the Rosetta(DE3) strain of *Escherichia coli* (EMD Millipore). Recombinant protein was passed over HisPur cobalt resin, and the His-tagged protein was eluted with 150 mM imidazole in 1× PBS, pH 8.5. Imidazole was removed by buffer exchange in a PD-10 column (GE Healthcare) before immunization. Polyclonal antibodies were raised in rabbits against His-*Op* vinculin (Syd Labs) and affinity-purified from serum using *E. coli* lysates to remove nonspecific antibodies and then His-*Op* vinculin recombinant protein to select for antigen-specific antibodies; both steps were conducted using AminoLink Plus Coupling Columns (Thermo Scientific) per the manufacturer's instructions.

For Western blotting analysis, frozen *O. pearsei* tissue was dissolved in Pierce IP lysis buffer containing protease inhibitor mixture (Roche). Cell debris was removed by centrifugation at 13,000 × *g* for 10 min. Lysate was mixed with 4× Laemmli sample buffer, and proteins were separated by SDS-PAGE. Proteins were transferred to a PVDF membrane, and membranes were blocked for 1 h at room temperature in 5% nonfat dry milk in 1× PBST (0.1% Tween 20), incubated with anti-*Op* vinculin antibody (1:10,000) in blocking solution for 1 h at room temperature, and washed twice in 1× PBST. After 45 min of incubation with secondary antibody (Alexa 488 goat anti-rabbit IgG antibody, from Life Technologies; 1:500) at room temperature, the membranes were washed in 1× PBST and developed using Molecular Imager FX ProPlus (Bio-Rad). Antibodies against His-*Op* vinculin recognized a single band of ~100 kDa and partially degraded protein. Preincubation of the antibody with competitor antigen (0.5 μg of His-*Op* vinculin) was used to confirm specificity.

Immunostaining of O. pearsei tissues

O. pearsei tissues were collected from aquaria at the University of California Santa Cruz where they grow naturally in the circulating sea water. Different fixation conditions were used for each adult tissue type. Choanoderm was fixed in 4% paraformaldehyde for 30 min at room temperature; the pinacoderm was fixed in 4% paraformaldehyde, 0.1 M phosphate buffer (EMS) for 1 h at room temperature. The samples were washed twice in 1× PBS and blocked for 1 h at room temperature with 3% BSA, 0.1% Triton in 1× PBS. Fixed tissues were incubated with primary anti-*Op* vinculin antibody (1:1000 to 1:2500 dilutions) in blocking buffer for 2 h at room temperature. The samples were washed three times with blocking buffer and then incubated for 45 min with Alexa 488 goat anti-rabbit IgG secondary antibody (1:500, from Life Technologies), with Alexa Fluor 568 phalloidin (1:100, Life Technologies), and Hoechst 33342 (1 μg/ml) at room temperature. The samples were washed three times in PBS and mounted on a FluoroDish plate for imaging using anti-quenching mounting medium.

Recombinant Op vinculin expression and purification

For SEC–MALS and crystallographic experiments, DNA encoding full-length (amino acids 1–846) *O. pearsei* vinculin was inserted into a pET His_6 Sumo TEV LIC vector (Addgene plasmid 29659, a gift from Scott Gradia). Fusion proteins of *Op* vinculin full-length, *Op* vinculin 1–257, and an N-terminal TEV-cleavable GSH-*S*-transferase tag were used for ITC and actin-binding experiments. Recombinant fusion proteins were expressed in BL21 (DE3) codon plus *E. coli* (Agilent Technologies). The cells were grown at 37 °C to an A_{600} of 0.8 and then induced with 0.1 M isopropyl-1-thio-β-D-galactopyranoside at 16 °C. After overnight growth, the cells were harvested by centrifugation and resuspended in 20 mM Tris, pH 8.0, 150 mM NaCl, 5 mM β-mercaptoethanol (His_6-tagged protein) or 1 mM DTT (GST-tagged protein) before storage at −80 °C. The cells were lysed in EmulsiFlex (Avastin) after addition of protease inhibitor mixture (Mixture Set V, Calbiochem), and lysates were cleared by centrifugation at 38,500 × *g* for 30 min. For purification of His_6–Sumo fusion protein, supernatant was incubated with nickel–nitrilotriacetic acid–agarose beads for 30 min at 4 °C. Beads were washed with 20 mM HEPES, pH 8.0, 150 mM NaCl, 1 mM β-mercaptoethanol and equilibrated for TEV cleavage in 20 mM HEPES, pH 8.0, 150 mM NaCl, 1 mM β-mercaptoethanol, 10% glycerol. Recombinant protein was incubated with TEV protease for 4 h at 4 °C to remove the His_6-Sumo tag. For purification of the GST-tagged proteins, supernatant after centrifugation was incubated with GSH-agarose beads for 30 min at 4 °C. The beads were washed with PBS containing 500 mM NaCl and 1 mM DTT and subsequently equilibrated with 20 mM HEPES, pH 8.0, 150 mM NaCl, 1 mM EDTA, 1 mM DTT, 10% glycerol. The protein was cleaved on the beads by overnight incubation with TEV at 4 °C. Cleaved proteins were eluted from beads and purified over a MonoQ anion exchange column with a 0–1 M NaCl gradient in 20 mM Tris, pH 8.0, 1 mM DTT. *Op* vinculin and vinculin 1–257 were further purified by Superdex 200 SEC in 20 mM HEPES, pH 8.0, 150 mM NaCl, and 1 mM DTT. Pure protein eluted as a monomer. The identity of purified vinculin 1–257 was further verified by MS after purification. Purified proteins were kept at 4 °C and used immediately for experiments.

Size-exclusion chromatography coupled to multiangle light scattering

The oligomeric state of full-length *Op* vinculin was assessed by SEC–MALS using a Superdex 200 column attached to a UV detector, followed by a DAWN EOS MALS detector and a refractive index detector (Wyatt Technology). The system was equilibrated with 20 mM HEPES, pH 8.0, 150 mM NaCl, and 2 mM DTT at 25 °C. Detectors were calibrated by measuring the signal of monomeric BSA. Molecular weights were calculated with ASTRA software (Wyatt Technology) using the signals from the MALS and the refractive index detectors.

Op vinculin crystallization and data collection

Purified full-length *Op* vinculin was concentrated to 60 mg/ml and crystallized in 0.2 M sodium/potassium tartrate, pH 8.0, 20% PEG 3350 using the sitting drop method and iterative

streak seeding. Plate-shaped crystals of approximate dimensions 350 × 60 × 5 μm grew in 4–5 days at 16 °C, were transferred to crystallization solution supplemented with 10% PEG 400 for cryoprotection, and frozen in liquid nitrogen. The diffraction data were measured in 0.2° rotation frames for 0.4 s/frame with a Pilatus 6M detector on Beamline 12-2 at the Stanford Synchrotron Radiation Laboratory. An initial data set used for molecular replacement extended to 2.83 Å, in the space group C2. Data for the final model refinement extended to 2.33 Å and were in space group P1. The data from the P1 crystal were measured from four different positions of a single long crystal, with 270, 280, 360, and 360° of rotation collected respectively at the four positions. The data were integrated with XDS (62) and scaled with AIMLESS in the CCP4 package (63). The data collection statistics are shown in Table S2.

Op vinculin structure determination and refinement

The structure of full-length *Op* vinculin was determined by molecular replacement in the C2 crystal form using a polyalanine model of the human vinculin structure (Protein Data Bank code 1TR2) (64) with residues 250–600 deleted, which was produced by MrBUMP (65). The structure was partially refined to R_{work}/R_{free} of 30%/35% through iterative cycles of manual rebuilding with the program Coot and positional, individual temperature factor and translation–libration–screw refinement in Phenix (66). Two copies of the partially refined structure in C2 were then found in the P1 form using the program Phaser (67) and further refined in Phenix. The final refinement statistics are provided in Table S2. The coordinates and structure factors have been deposited in the Protein Data Bank with accession code 6BFI.

High-speed actin co-sedimentation assays

Actin-binding assays were performed with 1.5 μM F-actin and increasing amounts of full-length *Op* vinculin (0.25–15 μM). Rabbit skeletal muscle G-actin (prepared as described in Ref. 68) was polymerized by addition of 10× polymerization buffer (100 mM Tris, pH 7.5, 20 mM $MgCl_2$, 500 mM KCl, 10 mM ATP) and incubated at room temperature for 1 h. Different vinculin concentrations were prepared by serial dilution starting from 20 and 30 μM vinculin, without or with 100 and 150 μM *Op* talin peptide, respectively (*i.e.* talin peptide at 5-fold molar excess) into assay buffer (20 mM HEPES, pH 8.0, 150 mM NaCl, 1 mM DTT, and 2 mM $MgCl_2$). After the addition of an equal volume of 3 μM F-actin or assay buffer, the mixture was incubated for 30 min at room temperature. An aliquot of each concentration point was removed as a standard. The samples were centrifuged at 60,000 rpm for 20 min at room temperature in a Beckman TLA 100 rotor. The pellet and the standard were separated by SDS-PAGE. Intensities of Coomassie-stained bands were quantified with an Odyssey imaging system (LI-COR Biotechnology). After background subtraction and normalization to the actin band, the concentration of pelleted vinculin was interpolated from the standard curve. The amount of bound vinculin per actin was plotted against the concentration of free vinculin using Prism software (GraphPad Software).

Synthetic peptide design

β-Catenin and talin peptides comprising the binding regions for α-catenin and vinculin, respectively, were designed based on homology to mammalian orthologs. Homology between *Mm* and *Op* β-catenin does not extend throughout the entire α-catenin–binding region but is limited to the minimal binding region of *Mm* αE-catenin spanning residues 118–149 (K_d = 377 nM) (69), which correspond to residues 233–266 in *Op* β-catenin (AIIGSPALIGGLVHVLGTTNDPDAMRSISGTLHN). The vinculin binding site of *Mm* talin comprises residues 605–628 (]K_d = 39 nM) (70). In a MUSCLE alignment *Mm* talin 605–628 correspond to residues 598–621 in *Op* talin (GEKLLEAARGLAGAVRHLLKSAEP). Both peptides were commercially synthesized with a N-terminal biotin tag and a five glycine linker (Genscript).

Isothermal titration calorimetry

ITC experiments were performed in a VP-ITC calorimeter (Microcal; GE Healthcare). 80–150 μM *Op* β-catenin or *Op* talin peptide was titrated into a solution of 6–10 μM *Op* vinculin 1–257 or full-length vinculin. One 2-μl injection was followed by 28 10-μl injections at 240-s intervals. Titrations were performed in 20 mM HEPES, pH 8.0, 150 mM NaCl, 1 mM DTT at 25 °C. For baseline correction, the heat change signals at saturation were averaged and subtracted from all data points. A one-site specific binding model was used to fit a binding curve (Microcal software; GE Healthcare). For the interaction of full-length *Op* vinculin and *Op* vinculin 1–257 with the *Op* talin peptide, binding data from three individual measurements were averaged to calculate the K_D, ΔH, and $T\Delta S$. Two measurements were performed for the *Op* vinculin 1–257–*Op* β-catenin interaction.

Author contributions—P. W. M., S. P., J. M. M., D. N. C., W. N., W. I. W., and S. A. N. conceptualization; P. W. M., J. V. C., and W. I. W. data curation; P. W. M., S. P., J. V. C., D. N. C., and W. I. W. formal analysis; P. W. M., S. P., J. M. M., D. N. C., and S. A. N. investigation; P. W. M., S. P., J. M. M., D. N. C., W. N., W. I. W., and S. A. N. visualization; P. W. M., S. P., J. M. M., and J. V. C. methodology; P. W. M., S. P., J. M. M., J. V. C., D. N. C., W. N., W. I. W., and S. A. N. writing-original draft; P. W. M., S. P., W. N., W. I. W., and S. A. N. writing-review and editing; S. P. and J. M. M. validation; W. N., W. I. W., and S. A. N. resources; W. N., W. I. W., and S. A. N. supervision; W. N. and W. I. W. funding acquisition; W. N., W. I. W., and S. A. N. project administration.

Acknowledgments—We thank Hadar Feinberg for assistance in the crystallographic analysis of Op vinculin, Betsy Steele for access to the Joseph Long Marine Laboratory (University of California Santa Cruz), and Christopher Lowe for use of confocal microscopy facilities at Hopkins Marine Station (Stanford University). Use of the Stanford Synchrotron Radiation Lightsource, SLAC National Accelerator Laboratory was supported by the U.S. Department of Energy, Office of Science, Office of Basic Energy Sciences under Contract DE-AC02-76SF00515. The SSRL Structural Molecular Biology Program is supported by the Department of Energy Office of Biological and Environmental Research, and by NIGMS, National Institutes of Health Grant P41GM103393).

References

1. Abedin, M., and King, N. (2010) Diverse evolutionary paths to cell adhesion. *Trends Cell Biol.* **20,** 734–742 CrossRef Medline
2. Niklas, K. J., and Newman, S. A. (2013) The origins of multicellular organisms. *Evol. Dev.* **15,** 41–52 CrossRef Medline
3. Knoll, A. H. (2011) The multiple origins of complex multicellularity. *Annu. Rev. Earth Planet. Sci.* **39,** 217–239 CrossRef
4. Harris, T. J., and Tepass, U. (2010) Adherens junctions: from molecules to morphogenesis. *Nat. Rev. Mol. Cell Biol.* **11,** 502–514 CrossRef Medline
5. Dumbauld, D. W., Lee, T. T., Singh, A., Scrimgeour, J., Gersbach, C. A., Zamir, E. A., Fu, J., Chen, C. S., Curtis, J. E., Craig, S. W., and García, A. J. (2013) How vinculin regulates force transmission. *Proc. Natl. Acad. Sci. U.S.A.* **110,** 9788–9793 CrossRef Medline
6. Harris, T. J., and Peifer, M. (2005) Decisions, decisions: β-catenin chooses between adhesion and transcription. *Trends Cell Biol.* **15,** 234–237 CrossRef Medline
7. Bryant, D. M., and Mostov, K. E. (2008) From cells to organs: building polarized tissue. *Nat. Rev. Mol. Cell Biol.* **9,** 887–901 CrossRef Medline
8. den Elzen, N., Buttery, C. V., Maddugoda, M. P., Ren, G., and Yap, A. S. (2009) Cadherin adhesion receptors orient the mitotic spindle during symmetric cell division in mammalian epithelia. *Mol. Biol. Cell.* **20,** 3740–3750 CrossRef Medline
9. Benham-Pyle, B. W., Pruitt, B. L., and Nelson, W. J. (2015) Cell adhesion: mechanical strain induces E-cadherin-dependent Yap1 and β-catenin activation to drive cell cycle entry. *Science.* **348,** 1024–1027 CrossRef Medline
10. Collins, C., and Nelson, W. J. (2015) Running with neighbors: coordinating cell migration and cell–cell adhesion. *Curr. Opin. Cell Biol.* **36,** 62–70 CrossRef Medline
11. Mui, K. L., Chen, C. S., and Assoian, R. K. (2016) The mechanical regulation of integrin–cadherin crosstalk organizes cells, signaling and forces. *J. Cell Sci.* **129,** 1093–1100 CrossRef Medline
12. Benjamin, J. M., and Nelson, W. J. (2008) Bench to bedside and back again: molecular mechanisms of α-catenin function and roles in tumorigenesis. *Semin. Cancer Biol.* **18,** 53–64 CrossRef Medline
13. Wilson, H. V. (1907) On some phenomena of coalescence and regeneration in sponges. *J. Exp. Zool.* **5,** 245–258 CrossRef
14. Humphreys, T. (1963) Chemical dissolution and in vitro reconstruction of sponge cell adhesions: I. isolation and functional demonstration of the components involved. *Dev. Biol.* **8,** 27–47 CrossRef Medline
15. Cauldwell, C. B., Henkart, P., and Humphreys, T. (1973) Physical properties of sponge aggregation factor: a unique proteoglycan complex. *Biochemistry* **12,** 3051–3055 CrossRef Medline
16. Henkart, P., Humphreys, S., and Humphreys, T. (1973) Characterization of sponge aggregation factor: a unique proteoglycan complex. *Biochemistry* **12,** 3045–3050 CrossRef Medline
17. Haseley, S. R., Vermeer, H. J., Kamerling, J. P., and Vliegenthart, J. F. (2001) Carbohydrate self-recognition mediates marine sponge cellular adhesion. *Proc. Natl. Acad. Sci. U.S.A.* **98,** 9419–9424 CrossRef Medline
18. Moscona, A. A. (1968) Cell aggregation: properties of specific cell-ligands and their role in the formation of multicellular systems. *Dev. Biol.* **18,** 250–277 CrossRef Medline
19. Grice, L. F., Gauthier, M. E. A., Roper, K. E., Fernàndez-Busquets, X., Degnan, S. M., and Degnan, B. M. (2017) Origin and evolution of the sponge aggregation factor gene family. *Mol. Biol. Evol.* **34,** 1083–1099 Medline
20. Vilanova, E., Santos, G. R., Aquino, R. S., Valle-Delgado, J. J., Anselmetti, D., Fernàndez-Busquets, X., and Mourão, P. A. (2016) Carbohydrate–carbohydrate interactions mediated by sulfate esters and calcium provide the cell adhesion required for the emergence of early metazoans. *J. Biol. Chem.* **291,** 9425–9437 CrossRef Medline
21. Halbleib, J. M., and Nelson, W. J. (2006) Cadherins in development: cell adhesion, sorting, and tissue morphogenesis. *Genes Dev.* **20,** 3199–3214 CrossRef Medline
22. Nelson, W. J. (2003) Adaptation of core mechanisms to generate cell polarity. *Nature* **422,** 766–774 CrossRef Medline
23. Plotnikov, S. V., Pasapera, A. M., Sabass, B., and Waterman, C. M. (2012) Force fluctuations within focal adhesions mediate ECM-rigidity sensing to guide directed cell migration. *Cell* **151,** 1513–1527 CrossRef Medline
24. Kanchanawong, P., Shtengel, G., Pasapera, A. M., Ramko, E. B., Davidson, M. W., Hess, H. F., and Waterman, C. M. (2010) Nanoscale architecture of integrin-based cell adhesions. *Nature* **468,** 580–584 CrossRef Medline
25. Buck, C. A., and Horwitz, A. F. (1987) Integrin, a transmembrane glycoprotein complex mediating cell–substratum adhesion. *J. Cell Sci.* **1987,** 231–250 CrossRef
26. Horwitz, A., Duggan, K., Buck, C., Beckerle, M. C., and Burridge, K. (1986) Interaction of plasma membrane fibronectin receptor with talin: a transmembrane linkage. *Nature.* **320,** 531–533 CrossRef Medline
27. Burridge, K., and Mangeat, P. (1984) An interaction between vinculin and talin. *Nature.* **308,** 744–746 CrossRef Medline
28. Turner, C. E., Glenney, J. R., Jr, and Burridge, K. (1990) Paxillin: a new vinculin-binding protein present in focal adhesions. *J. Cell Biol.* **111,** 1059–1068 CrossRef Medline
29. Tyler, S. (2003) Epithelium: the primary building block for metazoan complexity. *Integr. Comp. Biol.* **43,** 55–63 CrossRef Medline
30. Harwood, A., and Coates, J. C. (2004) A prehistory of cell adhesion. *Curr. Opin. Cell Biol.* **16,** 470–476 CrossRef Medline
31. Nickel, M., Scheer, C., Hammel, J. U., Herzen, J., and Beckmann, F. (2011) The contractile sponge epithelium sensu lato–body contraction of the demosponge *Tethya wilhelma* is mediated by the pinacoderm. *J. Exp. Biol.* **214,** 1692–1698 CrossRef Medline
32. Leys, S. P., and Hill, A. (2012) The physiology and molecular biology of sponge tissues. *Adv. Mar. Biol.* **62,** 1–56 CrossRef Medline
33. Adams, E. D., Goss, G. G., and Leys, S. P. (2010) Freshwater sponges have functional, sealing epithelia with high transepithelial resistance and negative transepithelial potential. *PLoS One* **5,** e15040 CrossRef Medline
34. Leys, S. P., Nichols, S. A., and Adams, E. D. (2009) Epithelia and integration in sponges. *Integr. Comp. Biol.* **49,** 167–177 CrossRef Medline
35. Nichols, S. A., Dirks, W., Pearse, J. S., and King, N. (2006) Early evolution of animal cell signaling and adhesion genes. *Proc. Natl. Acad. Sci. U.S.A.* **103,** 12451–12456 CrossRef Medline
36. Srivastava, M., Simakov, O., Chapman, J., Fahey, B., Gauthier, M. E., Mitros, T., Richards, G. S., Conaco, C., Dacre, M., Hellsten, U., Larroux, C., Putnam, N. H., Stanke, M., Adamska, M., Darling, A., *et al.* (2010) The Amphimedon queenslandica genome and the evolution of animal complexity. *Nature* **466,** 720–726 CrossRef Medline
37. Fahey, B., and Degnan, B. M. (2010) Origin of animal epithelia: insights from the sponge genome. *Evol. Dev.* **12,** 601–617 CrossRef Medline
38. Schippers, K. J., and Nichols, S. A. (2018) Evidence of signaling and adhesion roles for β-catenin in the sponge *Ephydatia muelleri*. *Mol. Biol. Evol.* **35,** 1407–1421 CrossRef Medline
39. Sebé-Pedrós, A., Roger, A. J., Lang, F. B., King, N., and Ruiz-Trillo, I. (2010) Ancient origin of the integrin-mediated adhesion and signaling machinery. *Proc. Natl. Acad. Sci. U.S.A.* **107,** 10142–10147 CrossRef Medline
40. Miller, P. W., Clarke, D. N., Weis, W. I., Lowe, C. J., and Nelson, W. J. (2013) The evolutionary origin of epithelial cell–cell adhesion mechanisms. *Curr. Top. Membr.* **72,** 267–311 CrossRef Medline
41. Dickinson, D. J., Nelson, W. J., and Weis, W. I. (2011) A polarized epithelium organized by β- and α-catenin predates cadherin and metazoan origins. *Science* **331,** 1336–1339 CrossRef Medline
42. Dickinson, D. J., Nelson, W. J., and Weis, W. I. (2012) An epithelial tissue in *Dictyostelium* challenges the traditional origin of metazoan multicellularity. *Bioessays* **34,** 833–840 CrossRef Medline
43. Boute, N., Exposito, J. Y., Boury-Esnault, N., Vacelet, J., Noro, N., Miyazaki, K., Yoshizato, K., and Garrone, R. (1996) Type IV collagen in sponges, the missing link in basement membrane ubiquity. *Biol. Cell.* **88,** 37–44 CrossRef Medline
44. Ereskovsky, A. V., Borchiellini, C., Gazave, E., Ivanisevic, J., Lapébie, P., Perez, T., Renard, E., and Vacelet, J. (2009) The homoscleromorph sponge *Oscarella lobularis*, a promising sponge model in evolutionary and developmental biology. *Bioessays* **31,** 89–97 CrossRef Medline

45. Nielsen, C. (2008) Six major steps in animal evolution: are we derived sponge larvae? *Evol. Dev.* **10,** 241–257 CrossRef Medline
46. Boury-Esnault, N., Ereskovsky, A., Bézac, C., and Tokina, D. (2003) Larval development in the Homoscleromorpha (Porifera, Demospongiae). *Invertebr. Biol.* **122,** 187–202 CrossRef
47. Nichols, S. A., Roberts, B. W., Richter, D. J., Fairclough, S. R., and King, N. (2012) Origin of metazoan cadherin diversity and the antiquity of the classical cadherin/β-catenin complex. *Proc. Natl. Acad. Sci. U.S.A.* **109,** 13046–13051 CrossRef Medline
48. Ereskovsky, A. V., Richter, D. J., Lavrov, D. V., Schippers, K. J., and Nichols, S. A. (2017) Transcriptome sequencing and delimitation of sympatric *Oscarella* species (*O. carmela* and O. pearsei sp. nov) from California, U.S.A. *PLoS One* **12,** e0183002 CrossRef Medline
49. Bateman, A., Coin, L., Durbin, R., Finn, R. D., Hollich, V., Griffiths-Jones, S., Khanna, A., Marshall, M., Moxon, S., Sonnhammer, E. L., Studholme, D. J., Yeats, C., and Eddy, S. R. (2004) The Pfam protein families database. *Nucleic Acids Res.* **32,** D138–D141 CrossRef Medline
50. Finn, R. D., Clements, J., and Eddy, S. R. (2011) HMMER web server: interactive sequence similarity searching. *Nucleic Acids Res.* **39,** W29–W37 CrossRef Medline
51. Letunic, I., Doerks, T., and Bork, P. (2012) SMART 7: recent updates to the protein domain annotation resource. *Nucleic Acids Res.* **40,** D302–D305 CrossRef Medline
52. Gasteiger, E., Hoogland, C., Gattiker, A., Duvaud S'everine Wilkins, M. R., Appel, R. D., and Bairoch, A. (2005) Protein identification and analysis tools on the ExPASy server. In *The Proteomics Protocols Handbook* (Walker, J. M., ed.) pp. 571–607, Humana Press, Totowa, NJ
53. Altschul, S. F., Madden, T. L., Schäffer, A. A., Zhang, J., Zhang, Z., Miller, W., and Lipman, D. J. (1997) Gapped BLAST and PSI-BLAST: a new generation of protein database search programs. *Nucleic Acids Res.* **25,** 3389–3402 CrossRef Medline
54. Larkin, M. A., Blackshields, G., Brown, N. P., Chenna, R., McGettigan, P. A., McWilliam, H., Valentin, F., Wallace, I. M., Wilm, A., Lopez, R., Thompson, J. D., Gibson, T. J., and Higgins, D. G. (2007) Clustal W and Clustal X version 2.0. *Bioinformatics* **23,** 2947–2948 CrossRef Medline
55. Camacho, C., Coulouris, G., Avagyan, V., Ma, N., Papadopoulos, J., Bealer, K., and Madden, T. L. (2009) BLAST+: architecture and applications. *BMC Bioinformatics* **10,** 421 CrossRef Medline
56. Capella-Gutiérrez, S., Silla-Martíinez, J. M., and Gabaldón, T. (2009) trimAl: a tool for automated alignment trimming in large-scale phylogenetic analyses. *Bioinformatics* **25,** 1972–1973 CrossRef Medline
57. Sánchez, R., Serra, F., Tárraga, J., Medina, I., Carbonell, J., Pulido, L., de María, A., Capella-Gutíerrez, S., Huerta-Cepas, J., Gabaldón, T., Dopazo, J., and Dopazo, H. (2011) Phylemon 2.0: a suite of web-tools for molecular evolution, phylogenetics, phylogenomics and hypotheses testing. *Nucleic Acids Res.* **39,** W470–W474 CrossRef Medline
58. Kalyaanamoorthy, S., Minh, B. Q., Wong, T. K. F., von Haeseler, A., and Jermiin, L. S. (2017) ModelFinder: fast model selection for accurate phylogenetic estimates. *Nat. Methods.* **14,** 587–589 CrossRef Medline
59. Trifinopoulos, J., Nguyen, L.-T., von Haeseler, A., and Minh, B. Q. (2016) W-IQ-TREE: a fast online phylogenetic tool for maximum likelihood analysis. *Nucleic Acids Res.* **44,** W232–W235 CrossRef Medline
60. Nguyen, L.-T., Schmidt, H. A., von Haeseler, A., and Minh, B. Q. (2015) IQ-TREE: a fast and effective stochastic algorithm for estimating maximum-likelihood phylogenies. *Mol. Biol. Evol.* **32,** 268–274 CrossRef Medline
61. Hoang, D. T., Chernomor, O., von Haeseler, A., Minh, B. Q., and Vinh, L. S. (2018) UFBoot2: improving the ultrafast bootstrap approximation. *Mol. Biol. Evol.* **35,** 518–522 CrossRef Medline
62. Kabsch, W. (2010) XDS. *Acta Crystallogr. D Biol. Crystallogr.* **66,** 125–132 CrossRef Medline
63. Winn, M. D., Ballard, C. C., Cowtan, K. D., Dodson, E. J., Emsley, P., Evans, P. R., Keegan, R. M., Krissinel, E. B., Leslie, A. G., McCoy, A., McNicholas, S. J., Murshudov, G. N., Pannu, N. S., Potterton, E. A., Powell, H. R., *et al.* (2011) Overview of the CCP4 suite and current developments. *Acta Crystallogr. D Biol. Crystallogr.* **67,** 235–242 CrossRef Medline
64. Borgon, R. A., Vonrhein, C., Bricogne, G., Bois, P. R., and Izard, T. (2004) Crystal structure of human vinculin. *Structure* **12,** 1189–1197 CrossRef Medline
65. Keegan, R. M., and Winn, M. D. (2008) MrBUMP: an automated pipeline for molecular replacement. *Acta Crystallogr. D Biol. Crystallogr.* **64,** 119–124 CrossRef Medline
66. Adams, P. D., Afonine, P. V., Bunkóczi, G., Chen, V. B., Davis, I. W., Echols, N., Headd, J. J., Hung, L.-W., Kapral, G. J., Grosse-Kunstleve, R. W., McCoy, A. J., Moriarty, N. W., Oeffner, R., Read, R. J., Richardson, D. C., *et al.* (2010) PHENIX: a comprehensive Python-based system for macromolecular structure solution. *Acta Crystallogr. D Biol. Crystallogr.* **66,** 213–221 CrossRef Medline
67. McCoy, A. J., Grosse-Kunstleve, R. W., Adams, P. D., Winn, M. D., Storoni, L. C., and Read, R. J. (2007) Phaser crystallographic software. *J. Appl. Crystallogr.* **40,** 658–674 CrossRef Medline
68. Spudich, J. A., and Watt, S. (1971) The regulation of rabbit skeletal muscle contraction I. Biochemical studies of the interaction of the tropomyosin-troponin complex with actin and the proteolytic fragments of myosin. *J. Biol. Chem.* **246,** 4866–4871 Medline
69. Pokutta, S., and Weis, W. I. (2000) Structure of the dimerization and β-catenin-binding region of α-catenin. *Mol. Cell* **5,** 533–543 CrossRef Medline
70. Bass, M. D., Patel, B., Barsukov, I. G., Fillingham, I. J., Mason, R., Smith, B. J., Bagshaw, C. R., and Critchley, D. R. (2002) Further characterization of the interaction between the cytoskeletal proteins talin and vinculin. *Biochem. J.* **362,** 761–768 CrossRef Medline
71. Clarke, D. N., Miller, P. W., Lowe, C. J., Weis, W. I., and Nelson, W. J. (2016) Characterization of the cadherin–catenin complex of the sea anemone *Nematostella vectensis* and implications for the evolution of metazoan cell–cell adhesion. *Mol. Biol. Evol.* **33,** 2016–2029 CrossRef Medline
72. Bakolitsa, C., de Pereda, J. M., Bagshaw, C. R., Critchley, D. R., and Liddington, R. C. (1999) Crystal structure of the vinculin tail suggests a pathway for activation. *Cell* **99,** 603–613 CrossRef Medline
73. Bakolitsa, C., Cohen, D. M., Bankston, L. A., Bobkov, A. A., Cadwell, G. W., Jennings, L., Critchley, D. R., Craig, S. W., and Liddington, R. C. (2004) Structural basis for vinculin activation at sites of cell adhesion. *Nature* **430,** 583–586 CrossRef Medline
74. Izard, T., Evans, G., Borgon, R. A., Rush, C. L., Bricogne, G., and Bois, P. R. (2004) Vinculin activation by talin through helical bundle conversion. *Nature.* **427,** 171–175 CrossRef Medline
75. Rangarajan, E. S., and Izard, T. (2013) Dimer asymmetry defines α-catenin interactions. *Nat. Struct. Mol. Biol.* **20,** 188–193 CrossRef Medline
76. Pokutta, S., Choi, H.-J., Ahlsen, G., Hansen, S. D., and Weis, W. I. (2014) Structural and thermodynamic characterization of cadherin·β-catenin·α-catenin complex formation. *J. Biol. Chem.* **289,** 13589–13601 CrossRef Medline
77. Shao, X., Kang, H., Loveless, T., Lee, G. R., Seok, C., Weis, W. I., Choi, H.-J., and Hardin, J. (2017) Cell–cell adhesion in metazoans relies on evolutionarily conserved features of the α-catenin·β-catenin–binding interface. *J. Biol. Chem.* **292,** 16477–16490 CrossRef Medline
78. Yamada, S., Pokutta, S., Drees, F., Weis, W. I., and Nelson, W. J. (2005) Deconstructing the cadherin–catenin–actin complex. *Cell* **123,** 889–901 CrossRef Medline
79. Benjamin, J. M., Kwiatkowski, A. V., Yang, C., Korobova, F., Pokutta, S., Svitkina, T., Weis, W. I., and James Nelson, W. J. (2010) αE-catenin regulates actin dynamics independently of cadherin-mediated cell–cell adhesion. *J. Cell Biol.* **189,** 339–352 CrossRef Medline
80. Kwiatkowski, A. V., Maiden, S. L., Pokutta, S., Choi, H.-J., Benjamin, J. M., Lynch, A. M., Nelson, W. J., Weis, W. I., and Hardin, J. (2010) *In vitro* and *in vivo* reconstitution of the cadherin–catenin–actin complex from *Caenorhabditis elegans*. *Proc. Natl. Acad. Sci. U.S.A.* **107,** 14591–14596 CrossRef Medline
81. Miller, P. W., Pokutta, S., Ghosh, A., Almo, S. C., Weis, W. I., Nelson, W. J., and Kwiatkowski, A. V. (2013) *Danio rerio* αE-catenin is a monomeric F-actin binding protein with distinct properties from *Mus musculus* αE-catenin. *J. Biol. Chem.* **288,** 22324–22332 CrossRef Medline

82. Ishiyama, N., Tanaka, N., Abe, K., Yang, Y. J., Abbas, Y. M., Umitsu, M., Nagar, B., Bueler, S. A., Rubinstein, J. L., Takeichi, M., and Ikura, M. (2013) An autoinhibited structure of α-catenin and its implications for vinculin recruitment to adherens junctions. *J. Biol. Chem.* **288,** 15913–15925 CrossRef Medline
83. Ziegler, W. H., Liddington, R. C., and Critchley, D. R. (2006) The structure and regulation of vinculin. *Trends Cell Biol.* **16,** 453–460 CrossRef Medline
84. Patel, B., Gingras, A. R., Bobkov, A. A., Fujimoto, L. M., Zhang, M., Liddington, R. C., Mazzeo, D., Emsley, J., Roberts, G. C., Barsukov, I. L., and Critchley, D. R. (2006) The activity of the vinculin binding sites in talin is influenced by the stability of the helical bundles that make up the talin rod. *J. Biol. Chem.* **281,** 7458–7467 CrossRef Medline
85. Rimm, D. L., Koslov, E. R., Kebriaei, P., Cianci, C. D., and Morrow, J. S. (1995) α1(E)-catenin is an actin-binding and -bundling protein mediating the attachment of F-actin to the membrane adhesion complex. *Proc. Natl. Acad. Sci. U.S.A.* **92,** 8813–8817 CrossRef Medline
86. Koslov, E. R., Maupin, P., Pradhan, D., Morrow, J. S., and Rimm, D. L. (1997) α-Catenin can form asymmetric homodimeric complexes and/or heterodimeric complexes with β-catenin. *J. Biol. Chem.* **272,** 27301–27306 CrossRef Medline
87. Pokutta, S., Drees, F., Takai, Y., Nelson, W. J., and Weis, W. I. (2002) Biochemical and structural definition of the l-afadin- and actin-binding sites of α-catenin. *J. Biol. Chem.* **277,** 18868–18874 CrossRef Medline
88. Drees, F., Pokutta, S., Yamada, S., Nelson, W. J., and Weis, W. I. (2005) α-Catenin is a molecular switch that binds E-cadherin-β-catenin and regulates actin-filament assembly. *Cell.* **123,** 903–915 CrossRef Medline
89. Choi, H.-J., Pokutta, S., Cadwell, G. W., Bobkov, A. A., Bankston, L. A., Liddington, R. C., and Weis, W. I. (2012) αE-catenin is an autoinhibited molecule that coactivates vinculin. *Proc. Natl. Acad. Sci. U.S.A.* **109,** 8576–8581 CrossRef Medline
90. Buckley, C. D., Tan, J., Anderson, K. L., Hanein, D., Volkmann, N., Weis, W. I., Nelson, W. J., and Dunn, A. R. (2014) Cell adhesion: the minimal cadherin–catenin complex binds to actin filaments under force. *Science* **346,** 1254211 CrossRef Medline
91. Bays, J. L., and DeMali, K. A. (2017) Vinculin in cell–cell and cell–matrix adhesions. *Cell. Mol. Life Sci.* **74,** 2999–3009 CrossRef Medline
92. Han, M. K., and de Rooij, J. (2016) Converging and unique mechanisms of mechanotransduction at adhesion sites. *Trends Cell Biol.* **26,** 612–623 CrossRef Medline
93. Carisey, A., and Ballestrem, C. (2011) Vinculin, an adapter protein in control of cell adhesion signalling. *Eur. J. Cell Biol.* **90,** 157–163 CrossRef Medline
94. Barstead, R. J., and Waterston, R. H. (1991) Vinculin is essential for muscle function in the nematode. *J. Cell Biol.* **114,** 715–724 CrossRef Medline
95. Barstead, R. J., and Waterston, R. H. (1989) The basal component of the nematode dense-body is vinculin. *J. Biol. Chem.* **264,** 10177–10185 Medline
96. Lecroisey, C., Ségalat, L., and Gieseler, K. (2007) The *C. elegans* dense body: anchoring and signaling structure of the muscle. *J. Muscle Res. Cell Motil.* **28,** 79–87 CrossRef Medline
97. Alatortsev, V. E., Kramerova, I. A., Frolov, M. V., Lavrov, S. A., and Westphal, E. D. (1997) Vinculin gene is non-essential in *Drosophila melanogaster*. *FEBS Lett.* **413,** 197–201 CrossRef Medline
98. Maartens, A. P., Wellmann, J., Wictome, E., Klapholz, B., Green, H., and Brown, N. H. (2016) *Drosophila* vinculin is more harmful when hyperactive than absent, and can circumvent integrin to form adhesion complexes. *J. Cell Sci.* **129,** 4354–4365 CrossRef Medline
99. Kang, H., Bang, I., Jin, K. S., Lee, B., Lee, J., Shao, X., Heier, J. A., Kwiatkowski, A. V., Nelson, W. J., Hardin, J., Weis, W. I., and Choi, H.-J. (2017) Structural and functional characterization of *Caenorhabditis elegans* α-catenin reveals constitutive binding to β-catenin and F-actin. *J. Biol. Chem.* **292,** 7077–7086 CrossRef Medline
100. Sarpal, R., Pellikka, M., Patel, R. R., Hui, F. Y., Godt, D., and Tepass, U. (2012) Mutational analysis supports a core role for *Drosophila* α-catenin in adherens junction function. *J. Cell Sci.* **125,** 233–245 CrossRef Medline
101. Costa, M., Raich, W., Agbunag, C., Leung, B., Hardin, J., and Priess, J. R. (1998) A putative catenin-cadherin system mediates morphogenesis of the *Caenorhabditis elegans* embryo. *J. Cell Biol.* **141,** 297–308 CrossRef Medline
102. Magie, C. R., Pinto-Santini, D., and Parkhurst, S. M. (2002) Rho1 interacts with p120ctn and α-catenin, and regulates cadherin-based adherens junction components in *Drosophila*. *Development* **129,** 3771–3782 Medline
103. Elliott, G. R., and Leys, S. P. (2007) Coordinated contractions effectively expel water from the aquiferous system of a freshwater sponge. *J. Exp. Biol.* **210,** 3736–3748 CrossRef Medline
104. Yonemura, S., Wada, Y., Watanabe, T., Nagafuchi, A., and Shibata, M. (2010) α-Catenin as a tension transducer that induces adherens junction development. *Nat. Cell Biol.* **12,** 533–542 CrossRef Medline
105. Humbert-David, N., and Garrone, R. (1993) A six-armed, tenascin-like protein extracted from the Porifera *Oscarella tuberculata* (Homosclerophorida). *Eur. J. Biochem.* **216,** 255–260 CrossRef Medline
106. Schuster, A., Vargas, S., Knapp, I., Pomponi, S. A., Toonen, R. J., Erpenbeck, D., and Woerheide, G. (2017) Divergence times in demosponges (Porifera): first insights from new mitogenomes and the inclusion of fossils in a birth-death clock model. *bioRxiv* CrossRef
107. Blumbach, B., Pancer, Z., Diehl-Seifert, B., Steffen, R., Münkner, J., Müller, I., and Müller, W. E. (1998) The putative sponge aggregation receptor: isolation and characterization of a molecule composed of scavenger receptor cysteine-rich domains and short consensus repeats. *J. Cell Sci.* **111,** 2635–2644 Medline